Cathodoluminescence for studies of low dimensional semiconductor structures

A Gustafsson

Solid State Physics/nm Structure Consortium
Lund University
Box 118, S-221 00 Lund, Sweden.

ABSTRACT: Cathodoluminescence (CL) is a very powerful technique for studying the optical properties of semiconductor structures, especially low-dimensional structures (structures with sub-micron features). We will give a number of examples of studies, where CL has been used to study a variety of low-dimensional semiconductor structures. We will also compare the CL technique with other techniques for studies of luminescence with high spatial resolution.

This is based on two invited papers. One was presented at "Microscopy of Semiconducting Materials XII" in Oxford in 2001, published in Institute of Physics conference Series and one was presented at "Electron Microscopy of Solids" in Kazimierz Dolny, Poland 2005, to be published in Journal of Microscopy.

1. INTRODUCTION

Until lately, CL has been unrivalled in luminescence studies with high spatial resolution. Over the last decade, a number of techniques with similar, or even higher spatial resolution have been developed. We will compare CL with other techniques for spatially resolved luminescence studies that we use in-house, i.e., micro photoluminescence (μPL) and scanning tunneling microscope induced luminescence.

1.1 The principles of CL

Luminescence is a process where a system (semiconductors in the present study) in an excited state emits photons in order to relax to a lower energy state. Many different methods of exciting the semiconductor are possible. Some examples of different methods are: sound (sonoluminescence), light (photoluminescence (PL)), heat (thermoluminescence), electron beams (CL), etc. Spatially resolved CL is usually performed using the focused electron-beam from a scanning electron microscope (SEM) or a scanning transmission electron microscope (STEM) (Yacobi and Holt 1986). As a consequence of the relaxation of the electrons of the beam, secondary electrons are formed, resulting in spreading of the excitation in the sample. This leads to the formation of an excitation volume, or generation volume, which can be substantially larger (depending mainly on the incident electron energy) than the beam diameter. The possibility to change the incident electron energy can be used to vary the penetration depth from a few tenths of a μm to several μm. The diffusion process of the created electron-hole-pairs or minority/majority carriers is also present, preventing extremely high resolution, but under favourable conditions the resolution can be better than 0.1 μm (Gustafsson et al 1998, Norman 2000).

The normal detection mode of the SEM/STEM, e.g. topographical imaging, electron beam induced current and X-ray emission, can be used to identify regions of interest, as well as, to avoid artefacts. Typical artefacts include dust particles or fragments of the substrate lying on the surface, and scratches and cracks on the surface. In combination with the normal secondary electron detection mode it is possible to locate specific areas

of the sample. This can for instance be an area of a quantum-well substrate that has been patterned by etching. In more complicated quantum structures, with emissions at several energies, monochromatic imaging and spot mode spectra can be used to identify the spatial origin of these peaks. The large range of available probe currents is useful for studying the excitation-density dependence of the emission peaks. The appearance of emission from excited sub-bands of quantum structures can be observed with increasing excitation densities. In the extreme case, the emission from single impurities can be identified and their position located (Samuelson and Gustafsson 1995).

One additional capability of CL is to vary the acceleration voltage of the SEM to obtain emission from different depths of the sample (the z-axis of the sample), where a higher voltage results in additional emission from a larger depth. In combination with the normal x-y (in-plane) resolution, it is possible to generate three-dimensional maps of the emission. It is not straightforward to interpret the data, due to a reduced in-plane (x-y) resolution with increasing acceleration voltage. To make things even more difficult, it is difficult to keep a constant excitation density in the sample, and the emissions may not be linear with excitation density. However, the general trends in variations along the z-axis are usually accessible (Gelhausen et al 2001).

1.2 Other techniques for high resolution luminescence studies

The most commonly used technique for studies of photon emission from semiconductors is the use of photons as the excitation source, PL. There are a number of available sources for excitation, and it is possible to choose the excitation energy to excite the whole sample, or to excite only low-energy parts. A typical example is when a quantum well (QW) is excited with an energy that is below the barrier, to have only direct excitation of the QW, without going through the complication of capture and relaxation from the barrier. It is also possible to tune the excitation to certain features of the electronic structure of the sample, e.g. an excited state in a QW. In a related technique, the energy of the excitation source is scanned, whereas the detection energy is fixed. This is known as PL excitation (PLE) and is used to identify the structure of the excited states of quantum structures, and to identify how the excitation is fed from adjacent structures. The excitation density can be varied by introducing neutral density filters into the excitation beam, virtually without affecting the spatial resolution. There are lasers with pulse widths of less than 1 ps, where it is possible to achieve an excitation by a single photon per pulse. As a comparison, a 100 pA electron beam contains _ 109 electrons per second, which is one electron per ns. This together with the fact that one electron generates several hundred electron-hole-pairs, puts some severe restrictions on the possibilities of time resolution of CL, although a resolution of 50 ps has been reported (Christen et al 1991).

As the excitation source is mainly a laser with a beam diameter of 50-500 μm, the spatial resolution was previously seriously limited. By including a simple focusing lens, it is possible to achieve a resolution of the order of 10 μm. The next step to increase the spatial resolution is to use a cryostat with an extremely short sample-to-window distance in combination with an optical microscope for the excitation and/or the light collection. This gives a spatial resolution of _1 μm, with the added advantage of a larger solid angle for light collection, meaning higher sensitivity and shorter integration times. To further improve the resolution and light collection efficiency, it is possible to put a solid immersion lens (SIL) directly on top of the sample (provided the surface is flat). This lens is generally a half sphere. This will take the resolution well into the sub-micron range. The combination of microscope and SILs are currently used in the PL set-ups at our division, with a spatial resolution of 100-200 nm. The ultimate in high spatial resolution

is to use scanning nearfield optical microscopy, with a potential spatial resolution of a few tens of nm (l/40 (Betzig et al 1991)). This system is however very complicated.

In the low-energy version of CL, a scanning tunnelling microscope (STM) is used to generate the electron beam. This technique is limited to conductive samples. Technically this is also CL, but to distinguish this technique from conventional CL, photon emission from the STM is generally referred to as scanning tunnelling luminescence (STL) In the STM, the bias voltage (acceleration voltage) can be varied from a few V to several hundreds of V. It is also possible to avoid the generation of electron-hole pairs. By switching the bias on the tip of the STM, it is possible to inject electrons or holes (extract electrons) into the sample. Due to the very local nature of the excitation, it is in principle possible to obtain a spatial resolution of the emission on the atomic scale. The low energy of the injected carriers means that it is possible to inject either electrons or holes directly into specific features of the electronic structure of the sample. This can be improved further by using a tip of a degenerately doped, large band-gap semiconductor, where the carriers in the tip are all within a narrow energy region near the band edge of the tip. This gives a more well-defined injection into the selected feature. The opposite may happen with a metal tip when, e.g. intending to inject electrons into the conduction band, there will also be some injection of electrons into the valence band. The low energy of the injected carriers implies that they have a short range in the sample. It is therefore important to have the features to study near the surface, in best cases just a few nm. The applied bias will affect the band bending of the sample. This has been observed in studies of quantum dots (QDs), where an increasing bias resulted in a shift in the energy position of the emission, due to the increasing electrical field, a Stark shift. The shift was more marked for QDs near the tip (Lindahl et al 1996).

The STL system used at our division is a combined ultra-high vacuum STM with an SEM for inspection and coarse positioning of the sample. The sample stage can be cooled to 20 K, using liquid helium. This gives the ability to compare STL and CL.

Although other techniques are improving on or even surpassing the spatial resolution of CL, the various techniques should be seen as complementing each other, rather than competing with each other.

1.3 instrumentation

As an example of a typical set-up we will show the one that is used by the authour in Lund, fig 1. This is based on a acannings electron microscope (SEM). The SEM itself is a Cambridge Instruments CI-250 mk III. It is equipped with an ion-pump for the option of using LaB_6 emitters, though we are currently using W-emitters. The vacuum system has been upgraded to a turbomolecular pump with magnetic bearings (Edwards) and a dry backing pump (Pfeifer). The gun has ben modified with a beamblanker (Kamrath & Weiss - originally Raith) capable of rise and fall times of 100 ps, using a pulse generator (Avtech or Techtronix). The stage has been replaced by a low-temperature stage, with a liquid He flow cryostat, capable of a base temperature of <5K (Gatan - originally Oxford Instruments). The SEM itself is controlled by an external computer, via the external scan interface of the instrument.

The cathodoluminescence system consists of a parabolic mirror placed above the stage, with the sampel in its focal plane. The resulting parallel light beam is transmitted through an optical window in the chamber wall and focussed onto the entrance slit of a monochromator (Spex). There is a range of detectors, whre the main ones are: GaAs photomultiplier (Hamamatsu in a housing) with either a current amplifier (Keithley) or a

photon counter (Stanford Reserach), lN_2-cooled Ge-detector (North Coast) with a lock-in amplifier (Stanford Reserach), lN_2-cooled Si CCD (Astromed). In addition, there are a number of simple fotodiodes, Si, Ge, InGaAs and InAS.

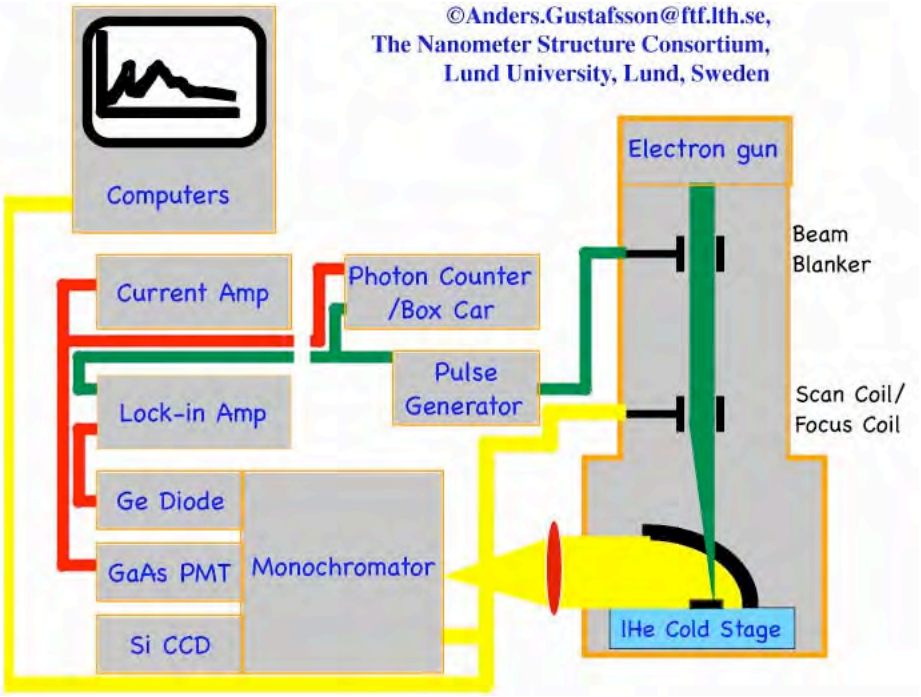

Fig. 1. A schematic of the set-up used in the author's lab in Lund.

2. EXAMPLES OF APPLICATIONS

We will give a number of examples where we have used CL to study various types of low-dimensional semiconductor structures. We will show results from GaP grown on masked Si substrates, intended for integration of optical devices into Si circuits. We will se how it is possible to study thickness variations in quantum wlls (QWs), both intentional in the form of growth on non-planar (V-grooved) substrates and shadow masked substrates and the unintentional form in flat QWs. One of the classic uses of spatially resolved CL is to study non-radiative recombination, and we will show examples of misfit dislocations in QWs of various materials systems, e.g., GaAsP in GaP. Strain, from lattice mismatch can be relaxed by the formation of three-dimensional islands, by Stranski-Krastanow (SK) relaxation. Since this is a cheap and reliable way to fabricate QDs in a reproducible way, these types of structures have attracted considerable attention lately. We will show luminescence data from InAs QDs, grown by the SK technique on the (110) sides of (001)-oriented GaAs substrates. We will also show examples, where the QW (InAs/InP) relaxes by both misfit dislocation and the QW (InAs/GaAs) relaxes by formation of more extended, flat islands. We will also show an example of the ultimate spatial resolution, where it is possibel to stydy the emission from single impurities in low-dimensional structures. Finally, we will show some results on degraded laser devices, in the form of QW based vertical cavity surface emitting lasers (VCSELs).

2.1 GaP grown on masked Si substrates

GaP grown on Si has a potential for device applications, e.g. heterojunction bipolar transistors, using the larger bandgap material of GaP as the emitter. The relatively large bandgap of the GaP also opens up possibilities of combining opto-electronic devices with Si substrates, e.g. visible light emitting diodes grown directly on a Si-based circuit. The growth of the samples in this study was done by chemical beam epitaxy (CBE). Under certain growth conditions in the CBE, it is possible to nucleate growth of the Ga sub-lattice only. Provided that the Si substrate is perfectly flat, or contains only ML-steps (i.e. no single Si steps), it will be possible to nucleate and grow anti-phase boundary (APB) free GaP. We have grown GaP crystallites in openings in masks of SiO_2 on (100) Si substrates. The openings were ≈200 nm in diameter

An SEM study (fig. 2b) reveals a variety in the shapes of the individual GaP crystallites. Some crystallites exhibit well developed facets, mainly (111) facets. This is expected for high quality growth, seeded from one point in the mask openings, or on a completely flat Si surface. Other crystallites exhibit more irregular shapes and a variety of facets. This is expected from multiply seeded crystallites or growth on a rough Si surface. A cross-sectional transmission electron microscopy study shows that there are differences between the Si surfaces below different crystallites. Some crystallites are grown on an uneven surface. This results in extended defects in the crystallites, probably related to APBs. In contrast, some crystallites are grown on a flat Si surface and appear to be free from the extended defects.

The low temperature CL spectra (fig. 2a) are dominated by a broad peak, related to Si-Si donor-acceptor pair (DAP) recombination, centered at 1.9 eV (Samuelson et al 1984). The Si in the GaP originates from the substrate. We can also identify the normal DAP emission at 2.2 eV and its phonon replica. Top view SEM images show differences in the shape of the GaP crystallites. Monochromatic CL images (fig. 2c) reveal a variation in the luminescence yield from different crystallites. It appears that crystallites with a more regular shape have a brighter emission intensity than more irregular ones. As discussed above, this may be related to the initial surface of Si, and thereby the presence of APB defects.

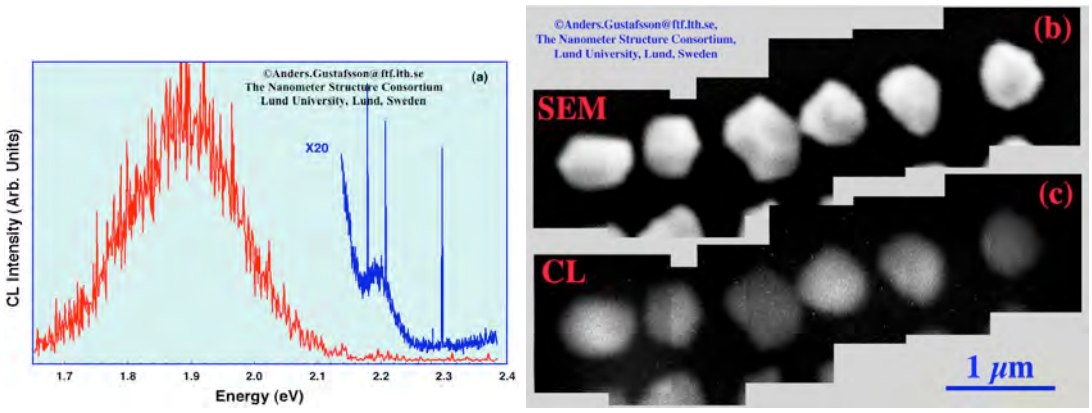

Fig. 2. a) A typical average spectrum from an area of 10X10 μm², recorded at 8.5K. b) The image is an SEM image, which illustrates the variety of the shape of the different GaP crystallites. c) a monochromatic CL image recorded at the same time as the SEM image using the 1.9 eV emission.

2.2 Thickness fluctuations in quantum wells

In very thin QWs, the difference in quantisation energy due to a thickness variation of one single atomic layer is large enough to distinguish the emission from different thicknesses (Gustafsson and Samuelson 1994). In III-V semiconductors, an atomic layer corresponds to a layer of the group III and the group V elements, a monolayer (ML). As it is almost impossible to fabricate a QW with absolutely flat interfaces; a QW is bound to have thickness fluctuations of at least one ML over a length scale of several tens of μm (Christen et al. 1991). I illustrate this by a sample containing several QWs of GaInAs lattice matched to the InP Barriers. Each QW has a different thickness and there is a gradient in the thickness along the direction of the gas flow in the MOCVD reactor. Fig. 3 shows a series of spectra recorded along the gradient, with a distance of 500 μm between two spectra in the series.

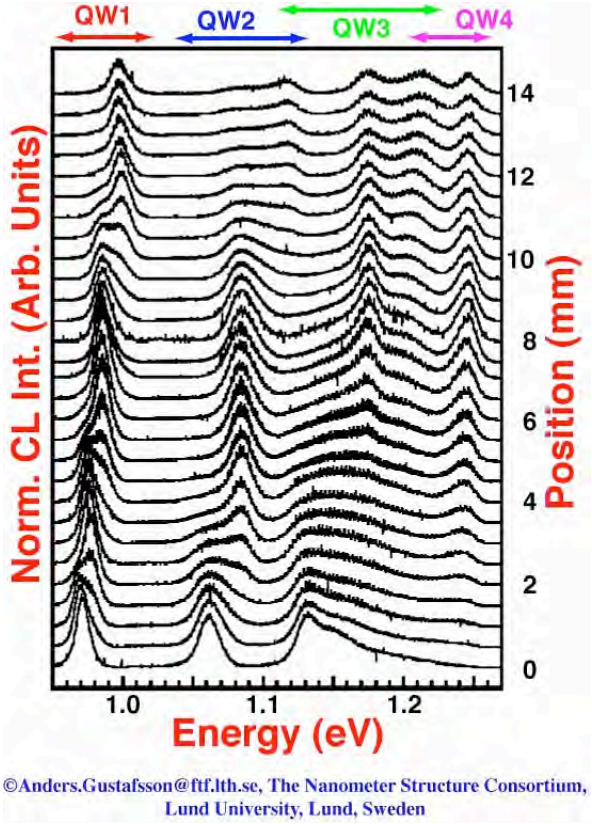

Fig. 3. A Series of spectra recorded along the thickness gradient

We concentrate on the QW with a thickness of 4-5 ML. The assignment of the thicknesses is not really important, but using the thickness gradient we were able to assign the emission peaks to different thicknesses. Fig. 4 shows a pair of top view images of the sample using the two emission peaks from the QW. The features of the images have similar extension, and they show complementary intensity variations, where one images is bright, the other one is dark, and so on. A simple interpretation of the images is that this is a map of the thicknesses in the QW.

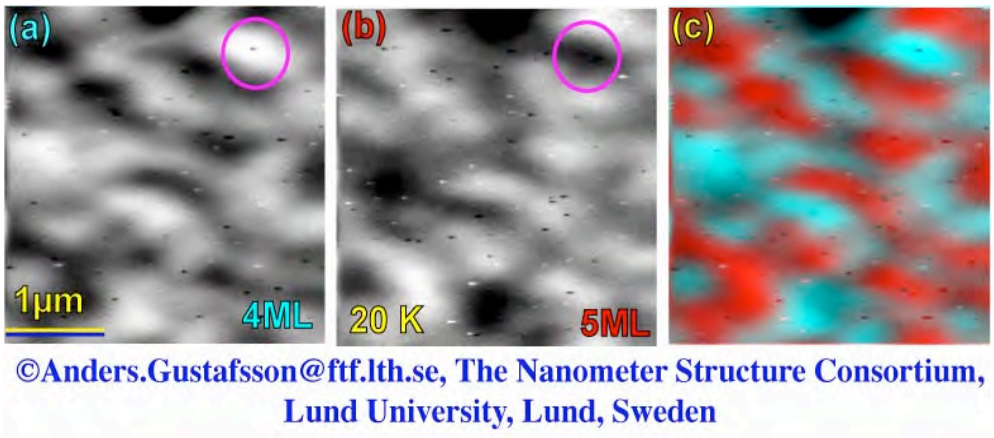

Fig. 4. Two monochromatic, top view images of a QW, corresponding to the emission from two different thicknesses of the same QW. a) is from a thickness of 4 ML and b) is 5ML. The purple circle indicates an area of complementary contrast. c) is a composite image, where (a) is shown in blue and (b) is shown in red.

A series of images recorded of the same area at increasing temperature (Fig. 5), shows that the interpretation is more complicated. With increasing temperature, the mobility of the carriers increase, thereby reducing the spatial resolution. Even though the features get increasingly fuzzy, the major features are still visible, and so is the complementarity between the two images. With increasing temperature, the size of complementary features increases, leading to an overestimation of the flat areas. We can conclude that the images are maps of a distribution of smaller areas of the two thicknesses rather than a direct map of the thickness. A bright area in one image means that that particular thickness dominates in that area.

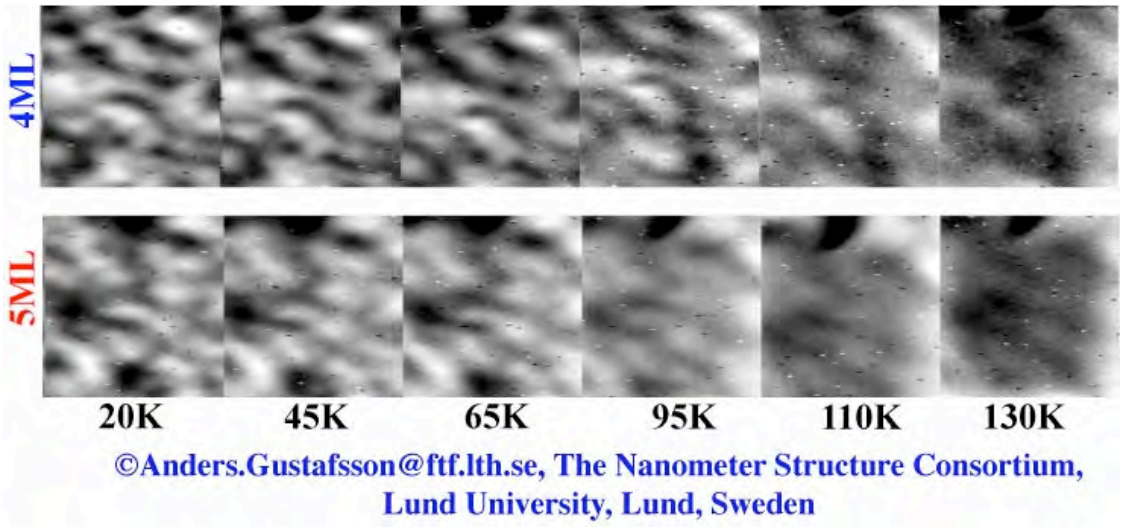

Fig. 5. A series of monochromatic images corresponding to fig. 4, with increasing temperature.

2.3 Misfit dislocations in quantum wells

A classic field for CL is the studies of dislocations in heterostructures, mainly III-V heterostructures. A necessary prerequisite for these types of studies is the knowledge of the behaviour and the luminescence properties of dislocations in general. Petroff et al. 1980 concluded that most types of dislocations act as non-radiative centres. A dislocation will therefore show up with a dark contrast in an image, either as a dark spot, if the dislocation is oriented perpendicular to the plane of the image or otherwise as a dark line. In mismatched heterostructures, the strain is released by the formation of misfit dislocations at the interfaces between the different materials. In a III-V QW structure, the first misfit dislocations generally originate from the threading dislocations, introduced into the epitaxial layers from the substrate. The segment of the threading dislocation inside the QW will move under the strain, producing a misfit dislocation at each interface along the path it moves. As threading dislocations generally lie on, and move on {111} planes, they will take a path along a <110> direction, resulting in dislocation lines along <110> directions, for growth on (001) substrates (Gustafsson et al 1991a and 1991b).

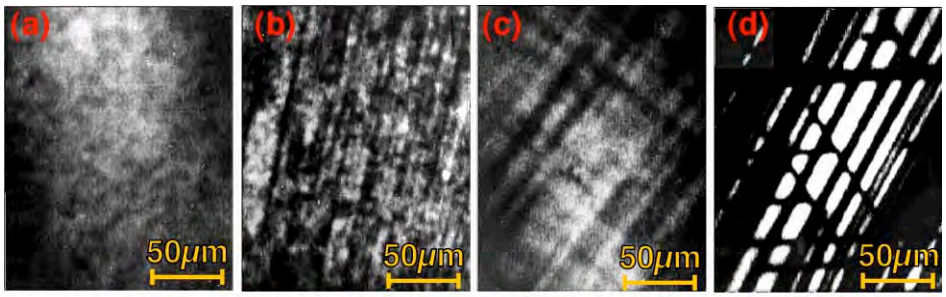

Fig. 6. A series of top view images of QWs a) only threading dislocations. b) misfit dislocations in one <110> direction. c) misfit dislocations in two orthogonal <110> directions. d) misfit dislocations in three <110> directions. All QW grown on (001) substrates except d, that was grown on a (111) substrate.

Our first example is a series of top view CL images (fig. 6), used to study the formation of misfit dislocations in GaP/GaPAs QWs, grown by metal-organic vapour phase epitaxy (MOCVD). The dislocation density was studied in a series of samples with varying thickness and composition of the QW. For growth on (001) substrates, the images exhibit three distinctly different patterns: i) QWs with minor strain shows only the dark spots of threading dislocations penetrating the plane of the QW. ii) QWs with medium strain shows a regular network of dark lines of misfit dislocations along one of the <110> directions in the (001) growth plane. iii) QWs with major strain shows a regular network of orthogonal dark lines of misfit dislocations along both <110> directions in the (001) growth plane. In addition, if the growth takes place on (111) substrates, the pattern is a regular network of dark lines in all three <110> directions in the (111) growth plane.

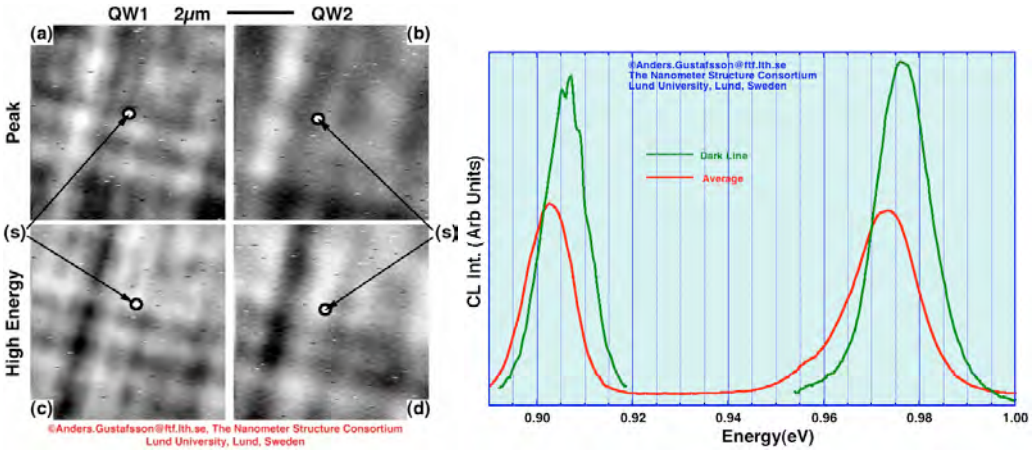

Fig. 7. Images using the peak energy position of the QWs a) and b) using the high energy side of the QW emission, c) and d). e) shows a set of spectra of the average emission and spot mode spectra from a dark spot in image a) and b).

It is however not always true that dark lines in the emission from a QW correspond directly to misfit dislocations in the QW. An example of this is illustrated (fig. 7) with a stack of three GaInAs QWs of different thickness, grown on (001) InP by MOCVD, in a sequence with the thickest QW first and the thinnest last. As the composition was slightly off lattice matching, the thicker QW exhibited a network of true misfit dislocations. This pattern was replicated in the top view images of peak energy position of the emission from the two thinner QWs (QW1 and QW2). If we recorded an image of the high-energy side of the emission from the two thinner QWs, the contrast was reversed. This tells us that the pattern of dark lines is related to the influence of the varying strain introduced by the misfit dislocations in the underlying thicker QW (QW3). It is worth mentioning that the thicker QW did not exhibit this contrast reversal.

2.4 Relaxation of strain by formation of 3-dimensional/misfit dislocations islands

As the misfit is increased, it gets energetically favourable for the layer to relax the strain by the formation of three-dimensional islands. This type of transition from the ordered two-dimensional (Frank-van der Merwe) growth is usually referred to as SK growth (Seifert et al 1996). In the first transition from the 2-D to 3-D growth, samples of a strained QW can exhibit a network of misfit dislocations, as well as, a low density of 3-D island. This is illustrated by a GaInAs/GaAs QW grown by CBE. This sample exhibits a low density of dark lines, corresponding to misfit dislocations, fig. 8b. It appears to be possible to follow the individual dislocations. The lines can also be observed as faint lines in the barrier emission, fig. 8a. At certain positions, there is a darker spot where a faint line ends. This probably corresponds to a position where the misfit segment of the dislocation joins its threading segment, as discussed above. The latter goes through the barrier rather than lies at the interface between the barrier and the QW, hence the higher contrast in the barrier emission. This sample also exhibit a very low density of 3D islands that can be found in the emission well below the energy of the QW, fig. 8c.

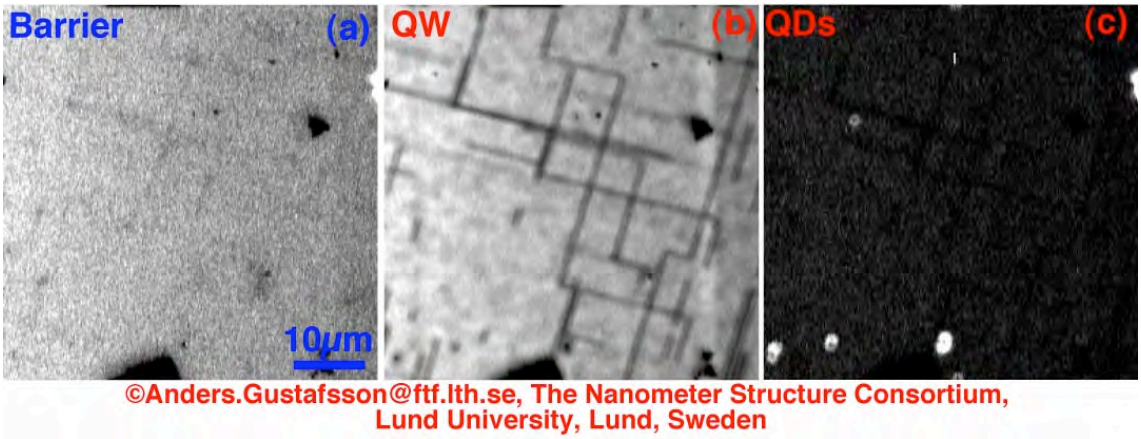

Fig. 8. A series of monochromatic images of a single QW structure, using a) the barrier, b) the QW, and c) the QD emission.

In the next step towards true SK growth, the strained QW breaks up into low, flat 3D islands, without any dislocation formation. This is illustrated by a sample of a thin layer of InAs grown on (001) InP by CBE (Gustafsson et al 1995). The average spectrum recorded over a 10×10 μm^2 area exhibits a large number of peaks, corresponding to a series of QWs with a thickness ranging from 1 ML to at least 10 ML of InAs, fig. 9a. The sensitivity of the detector in this case goes down significantly around 0.7-0.8 eV, which makes it hard to tell if there are any peaks beyond the 10 ML peak. The monochromatic images (fig. 9b and 9c) of all peaks from the QW all exhibit the same pattern of bright spots with an extension of 0.5 μm, which is the spatial resolution of the images, rather than the extension of the 3D-islands. TEM imaging of the sample places the in-plane extension of the islands to 5-50 nm, and it confirms the height to a few ML. It is worth pointing out that there are very few overlaps in the bright spots of the full series of images of all thicknesses and that there are no dark lines in pan-chromatic images.

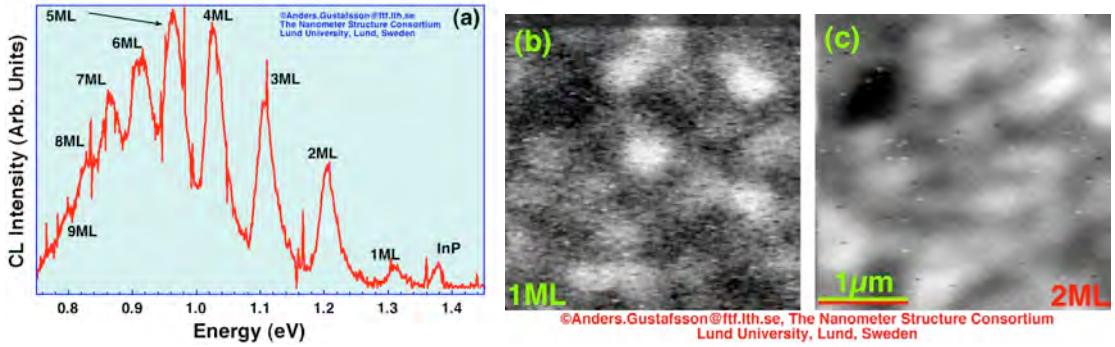

Fig. 9. a) an average (10×10μm^2) spectrum of a single QW sample. b) monochromatic images of using the b) 1 ML, and 2 ML peaks.

2.5 Stranski-Krastanow growth of GaInAs quantum dots on (110) GaAs

The signature of the SK growth mode is that the 3D-islands grow on top of a thin strained layer. Both the 3D-island and the strained layer are of similar composition. For SK growth of semiconductors the thin layer is termed the wetting layer and is normally just a few ML thick, but not necessarily a homogeneous or even fully covering layer. It is even possible that the formation of the 3D-islands consume the whole wetting layer for some distance surrounding it. Under most growth conditions, the 3D-islands are small enough to show quantization in all three dimensions, and not just in the growth direction. The islands can therefore be referred to as quantum dots. We illustrate the SK growth of QDs by a system, where InAs QDs are grown by CBE on the (110) (cleaved) side of (001) GaAs substrates. An interesting observation is that the growth is not fully flat as for normal (001) growth, but after the growth of the GaAs buffer layer, the surface exhibits a structure resembling fish scales, fig. 10a. This has been observed for (110) growth of GaAs before (Tajedor et al 1999). Concentrating on the wetting layer, we observe that the emission originates mainly from the flats of the fish scales and not at the edges. We can also notice thickness variations in the wetting layer when recording images from different positions of the emission peak, fig. 10c and 10d. This is consistent with a non-homogeneous wetting layer thickness. The images of the QDs, fig. 10b, exhibit a number of small bright spots corresponding to individual QDs. The image shown here is the sum of several images acquired for different energies and therefore correspond to a wide energy distribution of QDs. By recording spot mode spectra, we have been able to confirm that the spots correspond to what could be individual QDs, or in some cases two QDs close to each other. The broad emission peak of the QDs in the average spectrum of fig. 10e is an illustration of the spread in sizes of the individual QDs.

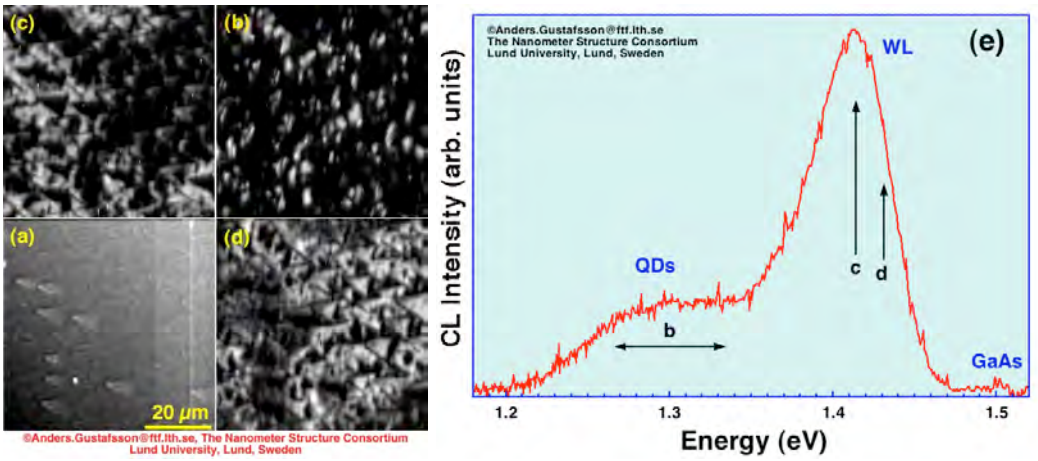

Fig. 10. A series of top view images of a single layer SK QD sample. a) is an SEM image and the rest are monochromatic images using b) the QD emission, c) the peak energy position and the high energy side of the wetting layer peak. e) is an average spectra.

2.6 Modification of quantum wells by shadow-masked growth

An example of intentionally induced thickness variations of QWs is to use a technique referred to as shadow-masked growth, where a mask with a limited opening is placed near the surface of the sample during growth. The width of the opening will determine the growth rate underneath the opening. the narrower the opening, the lower the growth rate. For a slit width of 5 μm the reduction in growth rate can be up to 3 times, using MOCVD growth (Vermeire 1994). By having a mask with a varying width, it is possible to manipulate the growth rate of a QW in a specific pattern. This can be used in device applications to vary the thickness of e.g. a light guide, connected to a stripe laser. By gradually narrowing the slit in the mask, the thickness of the QW in the light guide is reduced as the distance from the laser increases. The idea is to force the optical field out into the surrounding light confinement layer and thereby broadening the intensity distribution on the output facet, the near-field pattern. An increase in the size of the near-field pattern will reduce the far field distribution, mainly due to less slit-like diffraction from the facet. This can be used to improve the laser/fibre cupling.

The mask in the present case was held at a height of 7 μm above the waveguide and the width was reduced from 150 μm at the end of the laser stripe to 5 μm at the facet. The structure nominally consisted of a 5.6 nm thick GaInAs QW surrounded by 10 nm GaAs layers, in a AlGaAs graded refracting index (GRIN) structure, grown by MOCVD. Fig. 11 shows a line scan along the tapered light guide. As the electron beam is moved along the 200 μm long stripe, the energy is increased by 130 meV. This is mainly an effect of increased quantization due to the reduced thickness of the QW, but part of it can be related to a decrease in the In content of the QW towards the facet. As the confinement is increased, the intensity is also reduced. Part of this is caused by the mask, still present on the sample. This reduces the solid angle collected by the detection system. In the device the tapering of the output angle is reduced from 41° to 30° with a small reduction of the threshold current.

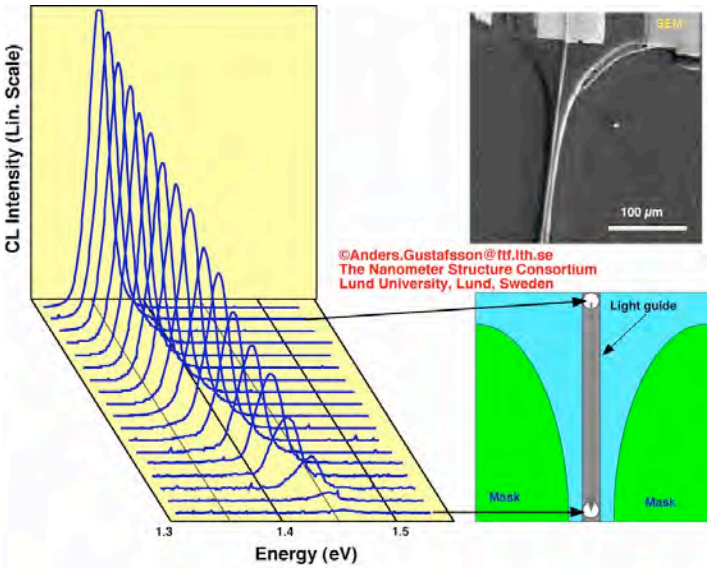

Fig. 11. a) a series of spot mode spectra, recorded along a tapered light guide. b) and SEM image of the structure and c) a schematic of the structure, indicating where the spectra were recorded.

2.7 Growth on V-grooved substrates

Thickness variations in QWs can be induced intentionally to form QWRs. One such method is growth on V-grooved substrates (Kapon et al 1989), which relies on the differences in growth rates on the various facets which define the V-groove. In the first stages of GaAs growth on a self-limiting, sharp AlGaAs V-groove, the growth rate at the bottom of the groove is higher than on the surroundings sidewalls. The resulting expansion of the facets at the bottom of the groove, together with the thickening in the growth direction, leads to the formation of a GaAs QWR, connected to thinner QWs on the side walls. The profile of the AlGaAs is only defined by the growth conditions and not by the initial shape of the V-groove, where the self-limiting profile of the AlGaAs is recovered after the growth of the GaAs layer. It is then possible to make a stack of identical QWRs.

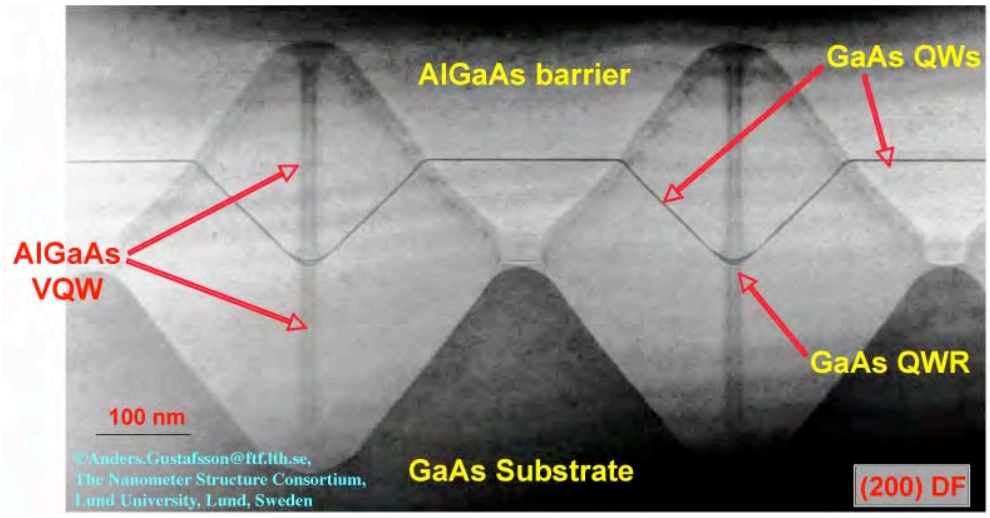

Fig. 12. A (002) dark field TEM image illustrating the growth on V-grooved substrates.

Fig. 12 shows an (002) dark-field TEM image of a single GaAs layer grown on a submicron grating of V-grooves. This is used as an illustration of the technique, as it is easier to obtain TEM images of the complete structure from short-period gratings. The original shape of the GaAs substrate can be observed as the dark lower part of the image and the AlGaAs is the lighter part above. The GaAs QW/QWR is the thin dark line in the AlGaAs layer. At this low magnification, it is possible to make out the slightly thicker GaAs at the bottom of the groove. Fig. 13 shows a series of CL images of a similar structure, but with a stack of ten QW layers and grown on grating with a 3.5 μm period. The CL images were recorded in side view. From the TEM images, it is clear that there are three distinct areas of the GaAs layer. The thicker region at the bottom of the groove, the sides of the grooves and the top of the ridges. The CL images reveal that the emission with the lowest energy (1.596 eV) originates at the bottom of the groove. Then follows the top of the ridges (1.658 eV) and the sides (1.729 eV). An interesting observation is that the emission energy of QWs on the side walls change with position. The QW is thicker further down in the groove and thinner high up the groove. TEM imaging of this sample confirms the trend in the QW thickness.

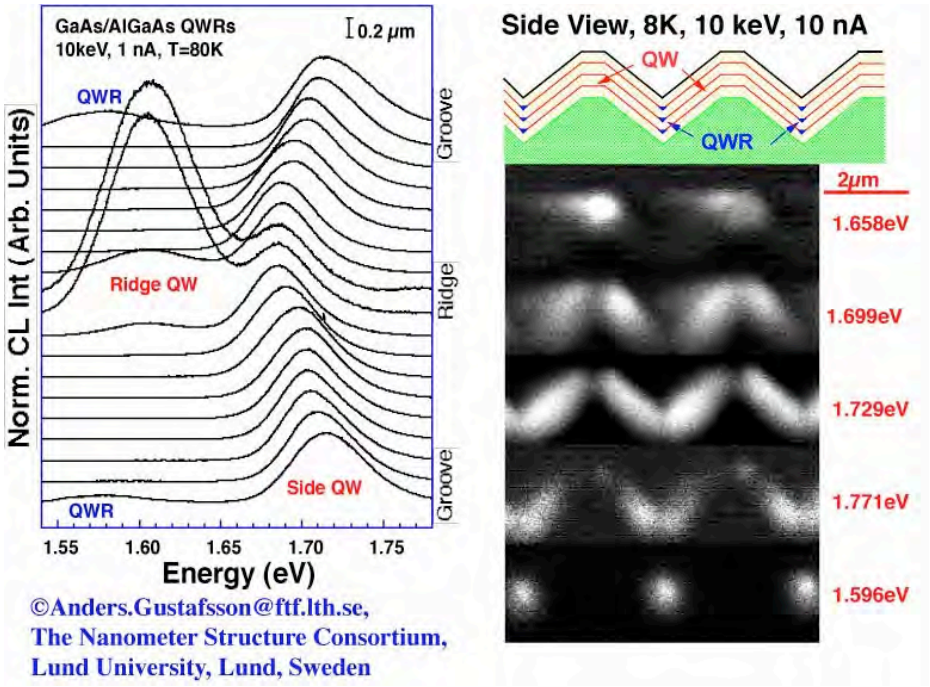

Fig. 13. A series of monochromatic, side view images of a stack of QWRs grown on a V-grooved substrate.

2.8 Nanowires, seeded by metal particles

A different approach to the fabrication of QWRs is to grow them, seeded from metal particles, using growth conditions when there is virtually no planar growth. The growth takes place at the interface between the metal particle and the semiconductor, where the growth takes its epitaxial information from the substrate (Ohlsson et al 2001). Often these structures are referred to as nano-whiskers. Here, I present data from nanowires with a core of GaAs and a shell of AlGaAs, grown with seed particles of gold by metal-organic chemical vapour depsition. Details of the growth conditions are presented elsewhere (Seifert et al 2004). The important parameter is the size of the particle, which determines the area of growth of the semiconductor underneath. This results in the growth of pillars with a very high aspect ratio. With a random size of the particles, the diameter of the pillars is also random. With a well-controlled size of the seed particles, the resulting pillars all have an identical diameter and identical height.

The nanowires shown here were grown to a typical length of 4 μm, using gold particles with a diameter of 40 nm. To avoid leaving the GaAs sides surfaces exposed, the nanowire cores were covered by a shell of AlGaAs, grown at higher a temperature. In contrast to the lower temperature of the core growth, growth takes place on the sides without the aid of metal particles. There is, however, still particle-mediated growth, forming an AlGaAs core at the top of the nanowire. This type of core-shell structure improves the light emission from the nanowires by 2-3 orders of magnitude in resonant (excitation below the band gap of the shell) photoluminescence studies. The thickness of the AlGaAs shell is about 55 nm, giving a total diameter of 150 nm.

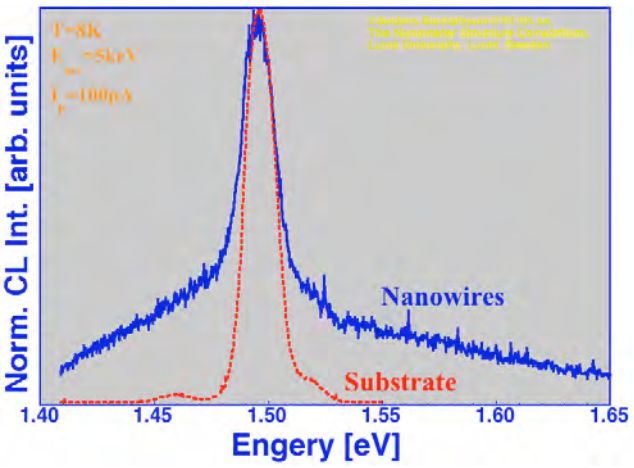

Fig. 14. Two spectra from a sample of nanowires seeded by metal particles. The substrate and the nanowires show similar features as the substrate, dominated by the emission from carbon acceptors.

Fig. 14 shows an average spectrum from a number of identical nanowires. The main spectral feature is a peak at 1.49 eV, related to carbon acceptors in GaAs. The 40 nm diameter of the structure is not small enough to introduce any significant energy shift from quantisation. There is also weak emission at 1.52 eV from excitons in the GaAs. Fig. 15 shows an SEM image (a) and the CL image (b) using the 1.49 eV emission, and (c) is a composite image of the two. An interesting feature of this emission is that it is much stronger from the top of the nanowire than from the bottom, as can be seen in fig. 15b. This is also the case for nanowires that have been broken off from the substrates. This rules out the transfer of carriers into the substrates or loss of emission due to waveguiding of the light into the substrate. The origin of the variation must be found in the nanowire itself. We have observed a number of stacking faults in nanowires grown under these conditions, which can influence the emission. During growth, there is believed to be significant transport of material from the substrate to the metal tip of the nanowire. This can leave residues at the core-shell interface, which can affect the emission efficiency. More studies are planned to understand the origin in the improved emission efficiency.

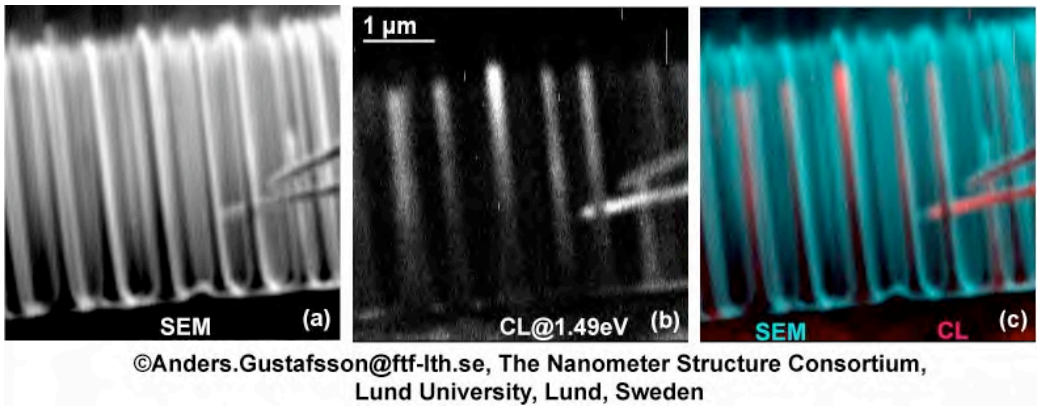

Fig. 15. Side view images of the same area of an sample of AlGaAs-covered GaAs nanowires. a) shows the SEM image and b) shows an image of the CL emission via the carbon acceptor in the nanowires. c) is a composite image of (a - blue) and (b - red).

The emission from the AlGaAs is not as well defined as there are a number of peaks in the range 1.53 - 1.80 eV. The emission peaks are related to different compositions. The spatial origin of the emission is not especially well defined, with the exception of the emission around 1.55 eV. This originates in the core of the nanowire, where the composition goes from GaAs to AlGaAs.

2.9 Individual impurities in low-dimensional structures

In most cases, the density of impurities is so high that there is no possibility to distinguish the effect of the individual impurities. Individual impurities are of interest when dealing with low dimensional structures. A sets of QDs can be designed to contain exactly one impurity per QD, where the individual QDs can contain zero, one or two impurities. This can alter the optical, as well as the electrical properties of the QDs, which can influence the performance of devices based on low-dimensional structures. We have previously shown that single impurities can be accessed by CL, using a special sample design (Samuelson and Gustafsson, 1995).

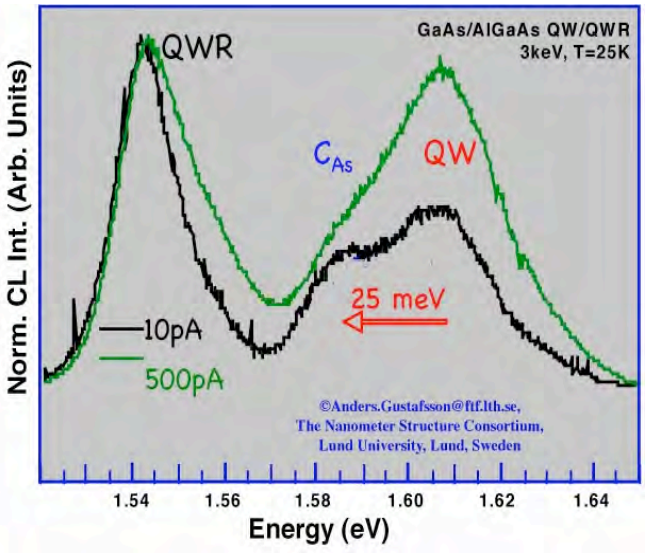

Fig. 16. Normalized CL spectra at different beam currents. The spectra have three features: QWR, QW and emission via a carbon acceptor in the QW.

The sample for this study is a single QWR grown in a V-grooved substrate, as described above. There are three main spectral features from the sample, fig. 16. The QWR at 1.54 eV, the planar QW at 1.61 eV and a peak at 1.59 eV that we attribute to recombination via carbon acceptors in the planar QW (Samuelson and Gustafsson, 1995). The corresponding top view images of the two QW-related peaks have one feature in common, the dark lines in the lateral position of the QWRs. The image of the carbon-acceptor emission shows a pattern of bright spots, corresponding to single acceptors, where it is possible to isolate the emission from single acceptors spectrally. The number of spots corresponds to the expected concentration of carbon in the QW, the emission is about 25 meV lower than the main QW emission and it saturates easily. The 25 meV would correspond to a thickness fluctuation of several MLs.

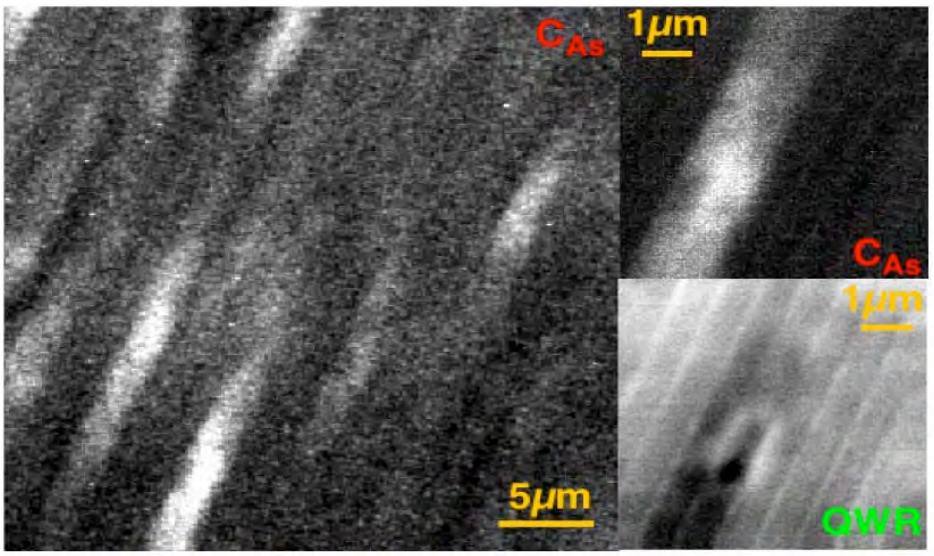

Fig. 17. Top view images of a sample of a single layer QWR, grown on a V-grooved substrate. The emission from the QWR is shown at one magnification and the emission from a single carbon acceptor the QWRs is shown at two different magnifications.

The same holds for the emission from the QWR, though the emission from the acceptors was to weak to observe spectrally. With the detection set to 25 meV below the main QWR peak, a number of bright spots are detected, about one per 5×5 μm^2. Fig. 17 shows two top view images. An interesting feature is the several μm extension of the spot along the QWR. This is an indication of the diffusion of carriers along the QWR. The extension across the QWR is limited by the centre of the adjacent V-grooves. In contrast to the higher carbon concentration of the metal-seeded nanowires, it is possible to identify the location of individual carbon impurities in these QWRs. One obvious reason is that these are much thinner, but it is likely that the concentration of carbon is significantly higher in the low-temperature growth of the nanowires.

2.10 Degradation of vertical cavity surface emitting lasers

A different type of optical device is a vertical cavity surface emitting laser (VCSEL) (Lear et al 1994). In this type of device, the active region is placed in between a pair of mirrors grown above and below it. As the name indicates, the light is emitted through the surface and not through the side facets like in a conventional laser. The mirror has a thickness of several μm and consists of a number of pairs of materials with different refractive indexes, typically AlGaAs/GaAs or GaInAsP/InP. These mirrors have a very high reflectivity (typically >99%) over a wide wavelength span, except for a very sharp dip in the reflectivity, the cavity mode. This mode is the only wavelength transmitted through the top mirror. It is the cavity mode, rather than the QW in the active area, that determines the wavelength of the emission from the laser. In this study, a series of AlGaAs VCSELs with QWs in the active region and a 20 μm output aperture, were put through ageing, using a higher than normal operating current and additional heating. This testing procedure may induce some defects that will degrade the emission from the VCSEL. In the CL study, we have investigated VCSELs that have shown signs of degradation. The typical degradation shows up as a gradual blinding of the emission from one side of the aperture. The blinding does not seem to follow any specific

crystallographic direction, as expected from a normal dislocation network. In order to be able to investigate the emission from the VCSELs, the major part of the top mirror must be removed, for two reasons: i) the thickness of the top mirror demands a very high acceleration voltage to excite the QWs. ii) more importantly, the top mirror only lets the cavity mode through, making it virtually impossible to study the true emission from the degraded QW.

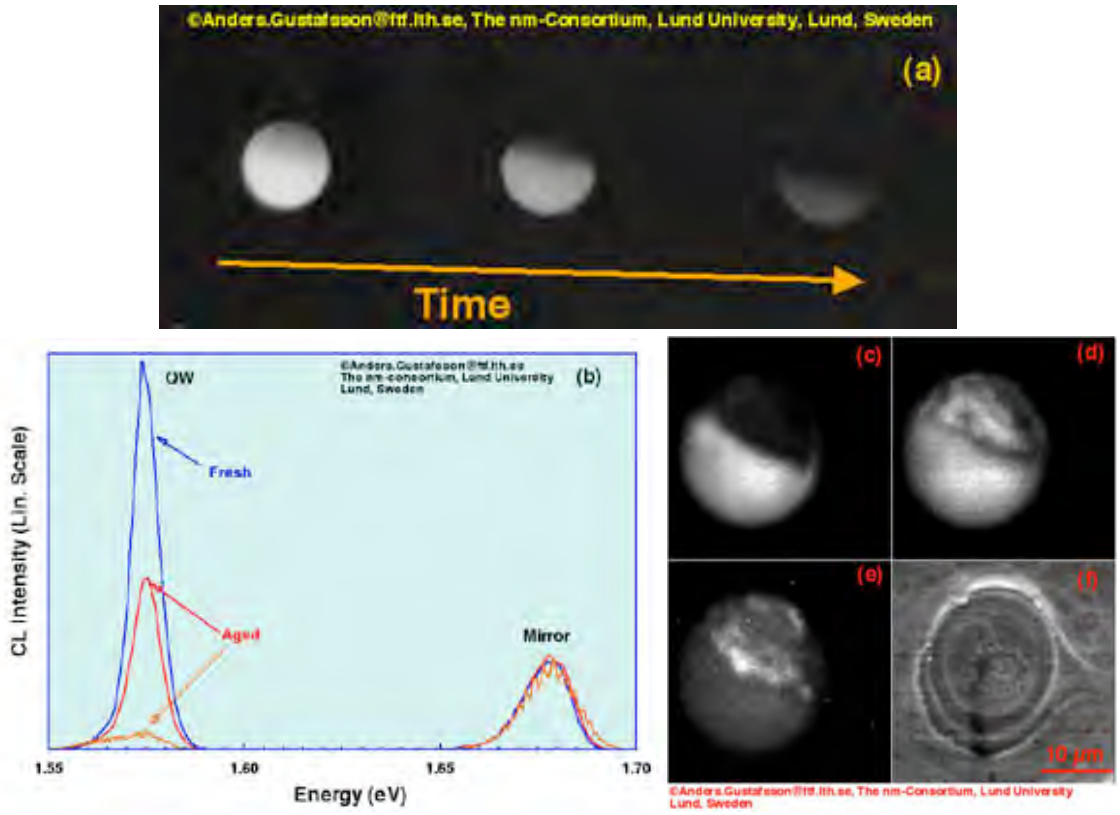

Fig. 18. a) electroluminescence images showing the gradual degradation of a VCSEL with time. b) CL spectra of the active area of three VCSELs (Fresh, minor degradation and major degradation). Monochromatic CL images of c) peak energy position, d) 10 meV and e) 25 meV on the low-energy side. f) an SEM image of the aperture of the VCSEL, after etching.

Fig. 18a shows the gradual blinding with time of the electroluminescence from one of the degraded devices. This compares well with the low-temperature CL data of fig. 18c. Using the emission peak from the QWs, the monochromatic images of the device look very much like the electroluminescence images after the ageing. This shows that the blinding is related to the optical properties of the active region and not to degradation of the electrical properties of the device. The images of the mirrors do not show any hint of the patterns of the blinding, implying that the damage only takes place in the active region. So far this points towards a network of dislocations forming during the ageing. However, when recording images on the high-energy side of the QW peak, the images show the same pattern, but when recording images on the low-energy side (fig. 18d and 18e) the pattern changes and where a weaker emission originates in the formerly dark region, indicating a red-shift of the emission from QW. This is not the normal pattern of the degradation of QWs, which would either be an introduction of dislocations, killing the emission, or an inter-diffusion of the QW and barrier, increasing the peak energy position of the QW. A way to reduce the emission energy is to introduce point defects in

the form of impurities/dopants. One possibility to achieve a significant reduction of the intensity and a red-shift at the same time is to introduce impurities, that will red-shift the emission as well as introduce non-radiative recombination in the form of e.g. Auger recombination. This could possibly be introduced by the passivation implantation used to electrically isolate the area surrounding the aperture in the device. More investigations are under way to further study the degradation process.

3. SUMMARY

We have illustrated some of the possibilities of the CL technique. In crystallites of GaP grown on Si, we have demonstrated a strong correlation by a regular shape and the emission intensity. We have illustrated various ways for a thin, strained layer to relax, by formation of misfit dislocations, extended 3D-islands, SK-islands and a combination of SK-islands and misfit dislocations. CL can be used to characterise optical devices, which we have demonstrated in the form of tapered waveguides and degraded VCSELs. We hope that we have demonstrated that there is still use for CL, despite the current development of other techniques for spatially resolved luminescene studies, i.e STL and μPL. The conclusion is that we should see the different techniques as complementing each other, rather than competing with each other

ACKNOWLEDGEMENTS

The various samples used in this study has been supplied from various sources and persons by S Andersson[a], P DeMeester[b], M Gerling[c,1], S Jeppesen[c], D Larsson[a], M R Leys[c,2], B J Ohlsson[c], A Rudra[d], W Seifert[c], H Titze[c], and G Vermeire[b,3]. Some of the data in the background material has been supplied by S Jeppesenc, M Johansson[c], U Håkansson[c], D Larsson[a], J Lindahl[c,4], J-O Malm[c].

[a]MITEL Sweden, [b]IMEC, Belgium, [c]Lund University Sweden, [d]EPFL, Lausanne Switzerland
[1]presently Nokia, Denmark, [2]presently Eindhoven University of Technology, The Netherlands, [3]presently Mietec, Belgium and [4]presently nQuip, Sweden.

The work has been performed with funding from, mainly, the nm-structure consortium in Lund, with support from national (e.g. TFR, NFR and NUTEK) and EU programmes.

The CL measurements were performed on the CL systems of Solid State Physics, Lund University and CIME, EPFL, Lausanne.

REFERENCES

Betzig E, Trautman J K, Harris T D, Weiner J S and Kostelak R L 1991 Science 251 1468

Christen J, Grundmann M and Bimberg D 1991 J. Vac. Sci. Technol. B 9 2358

Gelhausen O, Phillips M and Toth M 2001 J. Appl. Phys. 89 3535

Gustafsson A, Gerling M, Pistol M-E, Samuelson L, Leys M R and Titze H 1991a J. Appl. Phys. 70 1660

Gustafsson A, Gerling M, Pistol M-E, Samuelson L and Titze H 1991b J. Appl. Phys. 70 1667

Gustafsson A, Hessman D, Samuelson L, Carlin J F, Houdré R and Rudra A 1995 J. Crystal Growth 147, 27
Gustafsson A, Pistol, M-E, Samuelson L and Montelius L 1998 J. Appl. Phys. 84 1715
Gustafsson, A. & Samuelson, L. 1994 Phys. Rev. B50 11827-32
Kapon, E., Hwang, D.M. & Bhat, R. 1989 Phys. Rev. Lett. 63 430-3
Lear K L, Schneider R P, Choquette K D, Kilcoyne S P, Figeil J J and Zopler J C 1994 IEEE Photonics Technol. Lett. 6 1053
Lindahl J, Pistol M-E, Montelius L, Samuelson L 1996, Appl. Phys. Lett. 68 60
Norman C.E. 2000 Solid State Phenomena 78-79 19-25
Ohlsson, B.J., Bjork, M.T., Magnusson, M.H., Deppert, K. Samuelson, L. & Wallenberg, L.R. 2001 Appl. Phys. Lett. 79 3335-7
Petroff P M, Logan R A and Savage A 1980 Phys. Rev. Lett. 44 287
Samuelson L, Omling P and Grimmeiss H G 1984 J. Crystal Growth 68 340
Samuelson L and Gustafsson A 1995 Phys. Rev. Lett. 74 2395
Seifert, W., Borgström, M., Deppert, K., Dick, K.A., Johansson, J, Larsson, M.W., Mårtensson, T., Sköld, N., Svensson, C.P.T., Wacaser, B.A., Wallenberg, L-R. & Samuelson, L. 2004 J. Crystal Growth 272 211-20.
Seifert W, Carlsson N, Miller M S, Pistol M-E, Samuelson L and Wallenberg L R 1996 Progr. in Crystal Growth and Characterization 33 423
Tejedor P, Smilauer P, C. Roberts C and B. A. Joyce 1999 Phys. Rev. B 59, 2341
Vermeire G, Vermaerke F, Moerman I, Haes J, Baets R, van Daele P, Demeester P, Gustafsson A and Samuelson L 1994 J. Crystal Growth 145 875
Yacobi B G and Holt D B 1986 J. Appl. Phys. 59 R1.